DOE/NASA/50111-2
NASA TM-101439

Hot Corrosion of Ceramic Engine Materials

Dennis S. Fox, Nathan S. Jacobson, and James L. Smialek
National Aeronautics and Space Administration
Lewis Research Center

Work performed for
U.S. DEPARTMENT OF ENERGY
Conservation and Renewable Energy
Office of Vehicle and Engine R&D

Prepared for the
Twenty-sixth Automotive Technology Development
Contractors' Coordination Meeting
sponsored by the U.S. Department of Energy
Dearborn, Michigan, October 24-27, 1988

DISCLAIMER

Printed in the United States of America

Available from
National Technical Information Service
U.S. Department of Commerce
5285 Port Royal Road
Springfield, VA 22161

NTIS price codes[1]
Printed copy: A02
Microfiche copy: A01

[1]Codes are used for pricing all publications. The code is determined by the number of pages in the publication. Information pertaining to the pricing codes can be found in the current issues of the following publications, which are generally available in most libraries: *Energy Research Abstracts (ERA); Government Reports Announcements* and Index (*GRA* and I); *Scientific and Technical Abstract Reports (STAR).* and publication, NTIS-PR-360 available from NTIS at the above address.

DOE/NASA/50111-2
NASA TM-101439

Hot Corrosion of Ceramic Engine Materials

Dennis S. Fox, Nathan S. Jacobson, and James L. Smialek
National Aeronautics and Space Administration
Lewis Research Center
Cleveland, Ohio 44135

Work performed for
U.S. DEPARTMENT OF ENERGY
Conservation and Renewable Energy
Office of Vehicle and Engine R&D
Washington, D.C. 20545
Under Interagency Agreement DE-AI01-85CE50111

Prepared for the
Twenty-sixth Automotive Technology Development
Contractors' Coordination Meeting
sponsored by the U.S. Department of Energy
Dearborn, Michigan, October 24-27, 1988

HOT CORROSION OF CERAMIC ENGINE MATERIALS

Dennis S. Fox, Nathan S. Jacobson, and James L. Smialek
National Aeronautics and Space Administration
Lewis Research Center
Cleveland, Ohio 44135

SUMMARY

A number of commercially available SiC and Si_3N_4 materials were exposed to 1000 °C in a high velocity, pressurized burner rig as a simulation of a turbine engine environment. Sodium impurities added to the burner flame resulted in molten Na_2SO_4 deposition, attack of the SiC and Si_3N_4, and formation of substantial $Na_2O \cdot x(SiO_2)$ corrosion product. Room temperature strength of the materials decreased. This was a result of the formation of corrosion pits in SiC, and grain boundary dissolution and pitting in Si_3N_4. Corrosion regimes for such Si-based ceramics have been predicted using thermodynamics and verified in rig tests of SiO_2 coupons. Protective mullite coatings are being investigated as a solution to the corrosion problem for SiC and Si_3N_4. Limited corrosion occurred to cordierite ($Mg_2Al_4Si_5O_{18}$), but some cracking of the substrate occurred.

E-4544

INTRODUCTION

High temperature corrosion of hot section components becomes a concern when gas turbines are operated in corrosive environments. This process occurs when sodium, either as a fuel impurity or an airborne contaminant, combines with sulfur impurities in the fuel to form sodium sulfate by the following reaction:

$$2\ NaCl + SO_3 + H_2O = Na_2SO_4 + 2\ HCl \qquad (1)$$

Under certain conditions, liquid Na_2SO_4 condenses on hot-gas-path engine components. This leads to accelerated oxidation and severe corrosion. The hot corrosion of superalloys has been studied at length (refs. 1 to 3). The problem must also be addressed for ceramics, since these materials are being considered for heat engine components. In this paper, the results of a burner rig hot corrosion study of silicon carbide (SiC), silicon nitride (Si_3N_4), and cordierite ($Mg_2Al_4Si_5O_{18}$, or MAS) are presented. A burner rig was used because it models the high velocity, high temperature environment present in an operating turbine. Previous studies, reviewed in other publications, have shown SiC and Si_3N_4 to be quite susceptible to hot corrosion (refs. 4 to 8). A review of hot corrosion studies of cordierite is found in another publication (ref. 9).

At this point it would be helpful to discuss both the factors influencing hot corrosion and the reason a pressurized burner rig was used in this study. The deposition of Na_2SO_4 and subsequent corrosion is a function of temperature, pressure, sodium concentration, and sulfur concentration. In this study, conditions were chosen so that deposition occurs on the test specimens. Deposition of Na_2SO_4 and subsequent corrosion occurs in a temperature window bordered by the melting point of the salt (884 °C) and its dew point.

The NASA-CEC computer program (ref. 10) can be used to calculate dew points. The program, based on free energy minimization, is used to calculate combustion products. Inputs to the program are temperature, total system pressure, carbon/hydrogen ratio and sulfur content of the fuel, oxidant composition, and sodium concentration. When Jet A fuel (0.05 percent sulfur) is burned at 100 kPa (1 atm) total system pressure, with 2 ppm Na added to the flame, the dew point is 954 °C.

The high pressures encountered in turbine engines cause an increase in the dew point of Na_2SO_4, which expands the temperature range in which deposition and subsequent corrosion can occur. Raising the total system pressure to 400 kPa (4 atm) increases the dew point to 1020 °C for the same Jet A fuel and 2 ppm Na combination. The application of high pressure in this study produced the desired result of raising the dew point above the test temperature of 1000 °C. Current turbines operate at pressures from ~5 atm to ~20 atm. The temperature range for corrosion would therefore be even larger in practice because of higher dew points.

The burner rig corrosion of one type of sintered α-SiC has been previously studied by Jacobson et al. (ref. 11). A 4 atm burner rig fired with Jet A fuel was used, and 4 ppm sodium was aspirated into the flame. Samples were heated for 13.5 hr at 1000 °C, a temperature at which the corrosion kinetics are fast. A sodium silicate glass formed on the surface of the silicon carbide. Removal of this corrosion product revealed severe pitting. An average 32 percent reduction in room temperature bend strength was measured with respect to the as-received material. Jacobson and Smialek have studied the furnace corrosion of the same type of sintered α-SiC using thin, airbrush-applied salt films (refs. 4, 5, and 8). The chemical mechanism of attack and mode of strength degradation were basically the same for the furnace and burner rig studies.

Chemical mechanisms have been recently proposed for Na_2SO_4-induced corrosion of Si_3N_4 (refs. 6 and 12). It was found that the corrosion of Si_3N_4 occurs more slowly than that of SiC. This is due to the limited solubility of N_2 (versus CO) in the silicate. The presence of an Si_2N_2O diffusion barrier has also been suggested as a possible cause for this difference. Sintering additives in silicon nitride have a limited effect on the mechanism and kinetics.

The purpose of this study was to characterize the burner rig corrosion of a broad range of commercially available SiC and Si_3N_4 materials. A study to map corrosion regimes for such Si-based ceramics is also described, as is a project to determine the effectiveness of corrosion-resistant mullite coatings. Cordierite ($Mg_2Al_4Si_5O_{18}$), a possible regenerator material, was also investigated. These materials were investigated in the Advanced Gas Turbine (AGT) project (refs. 13 and 14). This paper summarizes the more detailed information found in three associated papers (refs. 9, 15, and 16).

CORROSION REGIMES

It has been shown that the hot corrosion of SiC and Si_3N_4 can be quite severe under certain conditions (refs. 4 to 8). Corrosion results from the dissolution of the protective silica layer found on the surface of these materials. SO_3 is a product of the reaction:

$$x\ SiO_2(s) + Na_2SO_4(l) = Na_2O \cdot x(SiO_2)(l) + SO_3(g) \quad (2)$$

It would be beneficial if one could determine under what conditions such dissolution occurs. This can be done using thermodynamics.

Na_2SO_4-induced corrosion regimes for SiO_2-protected ceramics have been calculated as a function of temperature, pressure, sodium concentration and sulfur concentration (ref. 16). The results are corrosion "maps" like those shown in figure 1, calculated for the NASA Mach 0.3 burner rig operating at 1000 °C and 4 atm with 2 ppm added Na. Both number 2 diesel (0.5 percent S) and Jet A (0.05 percent S) fuels were used.

First consider the horizontal axis, which indicates the temperature range for deposition of liquid Na_2SO_4. This occurs between the melting point of Na_2SO_4 (884 °C) and the dew point of the salt. As previously described, the NASA-CEC computer program is used to determine the dew point as a function of pressure, sodium concentration, and sulfur content of the fuel. The dew point is the highest temperature at which liquid Na_2SO_4 can condense.

Next consider the vertical axis, which describes the partial pressure of SO_3 required for dissolution. At high partial pressures of SO_3, the reaction will be forced to the left (eq. (2)). In this case, dissolution of SiO_2 would not occur. However, at lower partial pressures of SO_3, the reaction will proceed to the right as written, and corrosion will occur. Critical partial pressures at each temperature form the curved line marked with the circles. The area below this line, lying between the melting temperature and dew point of Na_2SO_4, is the predicted corrosion regime. These are the cross-hatched areas in figure 1. The partial pressure of SO_2 can also be used in the above calculations, although the same answer results.

The NASA-CEC program can then be used to determine the partial pressure of SO_3 above the deposit in the combustion (e.g., turbine engine) environment. This is plotted as the lines through the square markers in figure 1. Dissolution of the protective silica scale is predicted in the region where these lines intersect the corrosion regime. Similar diagrams have been generated for a variety of conditions (ref. 16). It has been found that corrosion regimes are limited. However, when corrosion does occur it can be quite severe, as will be discussed.

To substantiate the predictions, high purity SiO_2 (quartz) coupons were exposed in the burner rig. It should be noted that these specimens were purer than that which would form on SiC or Si_3N_4. At 1000 °C, the high partial pressure of SO_3 resulting from the use of number 2 diesel fuel is predicted to limit corrosion (point A in fig. 1(a) lies outside the regime). However, when low sulfur Jet A fuel is used, corrosion is predicted at 1000 °C (point B in fig. 1(b) lies inside the regime). These predictions were verified in the rig tests (ref. 16). Negligible dissolution took place in the former case, while considerable corrosion occurred in the latter.

EXPERIMENTAL PROCEDURE

The commercially available materials used in this study are listed in table I. The sintered cordierite samples were produced at NASA Lewis Research Center using a Ferro Corporation powder. Sample sizes were approximately 2.50

by 0.55 by 0.27 cm for SiC, 2.50 by 0.64 by 0.34 cm for Si_3N_4, and 2.50 by 0.50 by 0.25 cm for cordierite. The materials were corroded in the burner rig shown schematically in figure 2. The ends of the samples were held in grade A lava (alumino silicate) holders. The samples (4/run) were positioned horizontally with their thickness facing the flow. Jet A fuel (0.05 percent sulfur) was burned at a fuel-to-air ratio of 0.021 ± 0.002, producing a sample temperature of 1000 ± 5 °C. Corrosion kinetics are quite fast at this temperature (ref. 5). Sample temperature was measured with two Type R thermocouples. Gas velocity across the samples was 94 ± 3 m/sec (310 ± 10 ft/sec). Two ppm Na was added by aspirating a $NaCl/H_2O$ solution into the flame. The exposure time was 40 hr. The rig was pressurized to 400 kPa (4 atm) by closing down an exhaust control valve.

The morphology of the corrosion product was observed using scanning electron microscopy (SEM). An electron microprobe was used to determine its composition. The probe was equipped with a wavelength dispersive spectrometer which allowed oxygen mapping. Cross sections were prepared by sputter coating a thin layer of copper on the corroded samples, mounting them in epoxy and polishing them to a 1 μm finish with diamond. High-purity kerosene was used as a lubricant to preserve any water soluble phases present in the corrosion product. Trichloroethane was used as a solvent.

Chemical analysis was conducted on the corrosion product after it was removed from the samples. For SiC and Si_3N_4, this removal involved a 2 hr leach in hot (90 °C) water followed by a 2 hr leach in warm (60 °C) 10 percent HF/H_2O. For cordierite, a warm (60 °C) 50 percent HCl/H_2O was used. Elemental analysis of the solutions involved both inductively coupled plasma (ICP) atomic emission and X-ray fluorescence spectrometry.

To observe the attack morphology of the SiC substrate, the entire corrosion product was removed from a few corroded samples by dissolution in a hot (90 °C) 10 percent HF/H_2O solution for 2 hr. (Note that this etch differs from that in the preceding paragraph.) This solution cleanly removed the corrosion products and did not attack the SiC substrate.

In removing the corrosion product from the Si_3N_4 samples with HF, special care was required so as not to etch away any glassy grain boundary phases. An etch sequence was conducted on as-received samples polished to a 1 μm finish. This was to determine the correct time and temperature to be used in the treatment of the corroded Si_3N_4 samples. The chosen 10 percent HF etch conditions (60 °C, 15 min) revealed only a faint delineation of the grain boundaries in the as-received material. HF attacks cordierite, so a warm (60 °C, 2 hr) 50 percent HCl/H_2O solution was used to remove corrosion products from that material.

The room temperature strengths of both as-received and corroded SiC and Si_3N_4 were determined. A four point bend fixture having an outer span of 1.9 cm (0.75 in.) and an inner span of 0.95 cm (0.375 in.) was used. The loading rate was 0.05 cm/min (0.02 in./min). Since sample alignment in the test fixture is critical, the corrosion products were polished flat to provide a smooth sample surface on both the tensile and compressive sides. This was accomplished by polishing the samples with 600 grit SiC paper, followed by 45 and 15 μm diamond. A smooth layer of glass from 10 to 50 μm thick remained

after polishing. Fracture origins were observed by SEM. The cordierite samples were not strength tested.

RESULTS AND DISCUSSION

Silicon Carbide

The corrosion of the four types of SiC was very similar. The analysis of just one material, Carborundum Hexoloy sintered α-SiC, is therefore presented in detail. When this material is exposed in the burner rig with out adding sodium, it is unattacked according to visual examination. Figure 3 illustrates the result of a burner test on Hexoloy sintered α-SiC with 2 ppm sodium added. A substantial glassy corrosion product was formed after 40 hr at 1000 °C and 400 kPa pressure. The subsonic burner gases drive the corrosion product toward the trailing (or downstream) edge of the sample. This suggests that the corrosion product is liquid at 1000 °C. The glass was quite friable and spalled easily. Bubbles that are evolved and lead to the fragile nature of the corrosion product are seen macroscopically. A similar type of corrosion involving the formation of a friable, glassy corrosion product occurred with the three other SiC materials.

A mechanistic model for hot corrosion was developed in the previous burner rig study of Hexoloy α-SiC (ref. 11). Polished cross sections of the corroded material were examined using an electron microprobe. It was determined from the Si, O, and Na maps that the corrosion product consisted primarily of sodium silicate. Very low concentrations of sulfur were detected, indicating little Na_2SO_4 was present in the product layer. From these results and that of corresponding furnace tests (ref. 5), a reaction scheme for the Na_2SO_4 hot corrosion of SiC at 1000 °C has been determined. It is a continuous process involving oxidation of the carbide and dissolution of silica to form sodium silicate:

$$SiC(s) + 3/2\ O_2(g) = SiO_2(s) + CO(g) \quad (3)$$

$$x\ SiO_2(s) + Na_2SO_4(l) = Na_2O \cdot x(SiO_2)(l) + SO_3(g) \quad (4)$$

Equation (4) is thermodynamically favorable at low SO_3 partial pressures. The reaction proceeds to the right because SO_3 is purged by the Mach 0.3 burner gases. It is the evolution of CO and SO_3 that produces the bubbles observed in the corrosion product. Salt-enhanced oxidation of SiC occurs quite readily as compared to straight oxidation. This is because the corrosion product is liquid sodium silicate at 1000 °C, rather than solid silica.

The results of the room temperature strength tests on the four SiC materials are listed in table II. Figure 4 illustrates these results. The materials are ranked according to highest percentage of retained strength. The range of attack is due to various factors which include differing processing techniques, material morphologies, and additives. Note that the post-corrosion strengths of the first three types of SiC are nearly the same at about 300 MPa (44 ksi). The highest degree of strength reduction occurred in the injection molded siliconized KX01 material. Pure silicon initially corrodes much faster than SiC (ref. 12). It is possible that the free silicon in this material was preferentially attacked, resulting in the large strength decrease.

Hot corrosion enhances the oxidation of SiC due to the presence of liquid $Na_2O \cdot x(SiO_2)$. A fracture origin in corroded Hexoloy α-SiC is shown in figure 5(a). The enlargement (fig. 5(b)) shows the point of failure to be a leading edge surface pit formed during burner rig exposure. Glassy corrosion product fills the pit. This glass exhibits little load carrying capability compared to the SiC substrate. The strength of ceramics is quite dependent on flaw size. The observed corrosion pit is much larger than any intrinsic flaw and will degrade strength (refs. 8, 11, and 17). Removal of the glass with HF reveals the full extent of attack (fig. 5(c)). Note the 50 μm deep pit and exposed individual grains. Fractography of the other three SiC materials also revealed corrosion pits. These acted as the source of failure in 28 out of the total 35 samples examined.

Silicon Nitride

The burner rig hot corrosion of the three types of Si_3N_4 (table I) was very similar to that of SiC. A glassy corrosion product formed during rig testing and was blown toward the trailing edge of the samples by the high velocity burner gases. This again indicates the corrosion product is liquid at 1000 °C. The product was not as friable as that found on SiC, although gas bubbles (evident from fractography) did evolve during corrosion. Because the corrosion of the three types of Si_3N_4 was quite similar, just one material (GTE AY6) is discussed in detail.

Elemental maps of a polished cross section of corroded AY6 Si_3N_4 show the corrosion product to be primarily $Na_2O \cdot x(SiO_2)$. From these results, and that of Si_3N_4-Na_2SO_4 thin film furnace corrosion studies (ref. 12), the following reaction scheme has been determined:

$$Si_3N_4(s) + 3\ O_2(g) = 3\ SiO_2(s) + 2\ N_2(g) \quad (5)$$

$$x\ SiO_2(s) + Na_2SO_4(l) = Na_2O \cdot x(SiO_2)(l) + SO_3(g) \quad (6)$$

This mechanism is similar to that of SiC. Again, oxidation of the Si_3N_4 is enhanced because the corrosion product is liquid at 1000 °C. In this case N_2 rather than CO is evolved. It is the evolution of N_2 and SO_3 that creates the bubbles present in the corrosion product.

To determine attack morphology, the corrosion product was removed by mild treatment (15 min, 60 °C) in a 10 percent HF/H_2O solution. This was done carefully so as not to remove any grain boundary phase in the Si_3N_4. The attack morphology is quite different from that of SiC. There is an absence of the general pitting as was observed on the surface of corroded α-SiC. The major mode of attack is dissolution of the grain boundary phase. Similar attack occurred on the two other Si_3N_4 materials.

Room temperature strength tests were conducted on both as-received and corroded Si_3N_4 samples. The results are listed in table III and shown in figure 6. Note that all three materials exhibited an approximate 30 percent reduction in strength. Fracture origins were more difficult to find with the SEM because deep, hemispherical pits were not as prevalent in corroded Si_3N_4 as in SiC. Those pits that were observed were much wider and shallower. The residual glassy scale on the surface of a fractured AY6 sample is shown in figure 7(a). An enlargement of the shallow (30 μm deep) pit shows massive bubble

formation (fig. 7(b)), with Si_3N_4 needles visible after HF dissolution (fig. 7(c)). Similar observations were made for the other silicon nitride materials.

Cordierite

Corrosion of $Mg_2Al_4Si_5O_{18}$ is quite different than that of SiC or Si_3N_4 (ref. 9). Na_2SO_4 can react with not only SiO_2, but MgO and Al_2O_3 as well. Also note that oxidation will not be part of the reaction process.

Three cordierite samples were exposed in the burner rig using the same conditions as for the Si-based ceramics, except that number 2 diesel fuel (0.5 percent sulfur) was used. After 40 hr at 1000 °C with 2 ppm Na added, a deposit and possible corrosion was observed (fig. 8). A polished cross section of a corroded sample is shown in figure 9. Using electron microprobe analysis, the corrosion product was determined to have a layered structure. The top layer (~10 μm) appeared to be Mg_2SiO_4. The much thicker underlying layer (~100 μm) was determined to be $NaAlSiO_4$.

These results, plus that from chemical analysis and X-ray diffraction, have been used to determine the corrosion reaction:

$$2\ Na_2SO_4(l) + Mg_2Al_4Si_5O_{18}(s) = 4\ NaAlSiO_4(s) + Mg_2SiO_4(s) + 2\ SO_2(g) + O_2(g) \qquad (7)$$

Both cordierite and the solid reaction products are silicates. The reaction may therefore involve simple structural changes.

There was evidence of cracking, similar to that shown in figure 9, in all of the microstructures examined. These cracks extend through the corrosion scale to the substrate. This is a potential problem because the regenerator has a thin wall honeycomb structure. A possible explanation for this cracking is that sodium causes devitrification of grain boundary glass in the cordierite. This could lead to a new phase and cause volume expansion differences. Another possibility is that sodium sulfate penetrates the cordierite, causing cracks on cooling. Additional study of regenerator materials appears warranted.

PROTECTIVE COATINGS

A study is being conducted to determine the effectiveness of corrosion-resistant coatings applied to SiC and Si_3N_4. Mullite ($3Al_2O_3 \cdot 2SiO_2$) coatings are being applied to Hexoloy SiC samples by Solar Turbines, Inc., using plasma spraying. Mullite was chosen because of its limited reaction with Na_2SO_4. Another factor was its good thermal expansion match with SiC (5.1 versus 4.3×10^{-6}/°C). To date, one set of samples has been delivered to NASA Lewis for testing in the burner rig. Coating thickness ranged from 250 to 500 μm. The samples were tested (1000 °C, 4 atm, 2 ppm Na, number 2 diesel fuel) for 20 hr. Spalling of the coating and subsequent corrosion of the SiC occurred in some places. It is likely that salt penetration through residual porosity in the mullite was the cause. Good resistance to corrosion was noted where

the coating remained intact. This study is ongoing. Plasma spray parameters are currently being optimized to achieve more dense mullite coatings.

SUMMARY AND CONCLUSIONS

Burner rig testing for 40 hr at 400 kPa (4 atm) total system pressure, with 2 ppm Na added, results in deposition of sodium sulfate and corrosion of SiC and Si_3N_4 at 1000 °C. The continuous process involves oxidation of SiC or Si_3N_4 and dissolution of SiO_2 to form $Na_2O \cdot x(SiO_2)$. Accelerated scale growth occurs because the silicate is liquid at 1000 °C. Longer exposures would totally destroy the materials. Gas evolution (SO_3, CO, N_2) accounts for the formation of bubbles in the glassy scale. Extensive pitting causes strength reductions of ~30 percent in three types of SiC and ~50 percent in siliconized SiC. Chemical attack of grain boundary material and the formation of wide pits results in a strength reduction of ~30 percent for the three Si_3N_4 materials studied.

Sodium sulfate corrosion regimes have been calculated for SiO_2-protected ceramics such as SiC and Si_3N_4. This information can be used as guidance for turbine designers. Mullite is being investigated as a protective coating for SiC. This shows promise as a possible solution to the corrosion problem. The corrosion of a regenerator material (cordierite) was also studied, and limited reaction was found to occur with Na_2SO_4. Cracking is observed in the material after rig exposure.

In conclusion, it is clear that Na_2SO_4-induced hot corrosion is a serious problem for ceramics in certain combustion applications. Engine designers should therefore be aware of this problem and its possible occurrence.

REFERENCES

1. Pettit, F.S.; and Meier, G.H.: Oxidation and Corrosion of Superalloys. Superalloys, M. Gell, et al., eds., The Metallurgical Society of AIME, Warrendale, PA, 1984, pp. 651-687.

2. Goebel, J.A.; Pettit, F.S.; and Goward, G.W.: Mechanisms for the Hot Corrosion of Nickel-Base Alloys. Metall. Trans., vol. 4, no. 1, Jan. 1973, pp. 261-278.

3. Stringer, J.: Hot Corrosion of High Temperature Alloys. Properties of High Temperature Alloys, Z.A. Foroulis, and F.S. Pettit, eds., The Electrochemical Society, Princeton, NJ, 1976, pp. 513-556.

4. Jacobson, N.S.; and Smialek, J.L.: Hot Corrosion of Sintered Alpha-SiC at 1000 °C. J. Am. Ceram. Soc., vol. 68, no. 8, Aug. 1985, pp. 432-439.

5. Jacobson, N.S.: Kinetics and Mechanism of Corrosion of SiC by Molten Salts. J. Am. Ceram. Soc., vol. 69, no. 1, Jan. 1986, pp. 74-82.

6. Fox, D.S.; and Jacobson, N.S.: Molten Salt Corrosion of Silicon Nitride: I - Sodium Carbonate. J. Am. Ceram. Soc., vol. 71, no. 2, Feb. 1988, pp. 127-138.

7. Palko, J.E.: A Review of Oxidation and Corrosion of Silicon Based Ceramics. Report No. 77-GTD-55, Technical Information Series, Gas Turbine Division, General Electric Co., Schenectady, NY, 1977.

8. Smialek, J.L.; and Jacobson, N.S.: Mechanism of Strength Degradation for Hot Corrosion of Alpha-SiC. J. Am. Ceram. Soc., vol. 69, no. 10, Oct. 1986, pp. 741-752.

9. Bianco, R.; and Jacobson, N.S.: Corrosion of Cordierite Ceramics by Sodium Sulfate. J. Mater. Sci., 1988, accepted for publication.

10. Gordon, S.; and McBride, B.J.: Computer Program for Calculation of Complex Chemical Equilibrium Compositions, Rocket Performance, Incident and Reflected Shocks, and Chapman-Jouguet Detonations. NASA SP-273, 1976.

11. Jacobson, N.S.; Stearns, C.A.; and Smialek, J.L.: Burner Rig Corrosion of SiC at 1000 °C. Adv. Ceram. Mater., vol. 1, no. 2, Apr. 1986, pp. 154-161.

12. Jacobson, N.S.; Fox, D.S.: Molten Salt Corrosion of Silicon Nitride: II - Sodium Sulfate. J. Am. Ceram. Soc., vol. 71, no. 2, Feb. 1988, pp. 139-148.

13. Proceedings of the Twenty-Fourth Automotive Technology Development Contractor's Coordination Meeting, SAE P-197, Society of Automotive Engineers, 1986.

14. Richerson, D.W.: Evolution in the U.S. of Ceramic Technology for Turbine Engines. Am. Ceram. Soc. Bull., vol. 64, no. 2, Feb. 1985, pp. 282-286.

15. Fox, D.S.; and Smialek, J.L.: Burner Rig Hot Corrosion of Ceramic Engine Materials. To be submitted to the J. Am. Ceram. Soc., 1989.

16. Jacobson, N.S.: Sodium Sulfate and Dissolution of Silica. Oxid. Met., vol. 30, nos. 5/6, 1988. (To be published.)

17. Jacobson, N.S.; and Smialek, J.L.: Corrosion Pitting of SiC by Molten Salts. J. Electrochem. Soc., vol. 133, no. 12, Dec. 1986, pp. 2615-2621.

TABLE I. MATERIALS

Silicon carbide	Silicon nitride
Carborundum Hexoloy SASC General Electric β-SiC Kyocera SC 201 Carborundum KX01	GTE AY6 Toshiba SSN NGK SN50 SSN
	Ferro Cordierite (MAS)

TABLE II. - ROOM TEMPERATURE STRENGTHS OF AS-RECEIVED AND CORRODED SiC

Type	As-received			After corrosion[a]			Strength reduction, percent
	Number of bars	Mean MOR		Number of bars	Mean MOR		
		MPa±σ[b]	ksi±σ		MPa±σ	ksi±σ	
Carborundum Hexoloy SASC	5	401±55	58±8	7	308±42	45±6	23
General Electric β-SiC	5	406±27	59±4	13	297±50	43±7	27
Kyocera SC 201	5	451±31	65±4	12	299±46	43±7	33
Carborundum KX01	5	431±61	63±9	15	206±94	30±14	51

[a]Mach 0.3 rig, 1000 °C, 40 hr, 400 kPa pressure, 2 ppm Na.
[b]Where σ is one standard deviation.

TABLE III. - ROOM TEMPERATURE STRENGTHS OF AS-RECEIVED AND CORRODED Si_3N_4

Type	As-received			After corrosion[a]			Strength reduction, percent
	Number of bars	Mean MOR		Number of bars	Mean MOR		
		MPa±σ[b]	ksi±σ		MPa±σ	ksi±σ	
GTE AY6	5	668±36	97±5	7	509±78	74±11	24
Toshiba	5	872±67	126±10	12	627±103	91±15	28
NGK SN50	5	814±55	118±8	13	547±116	79±17	33

[a]Mach 0.3 rig, 1000 °C, 40 hr, 400 kPa pressure, 2 ppm Na.
[b]Where σ is one standard deviation.

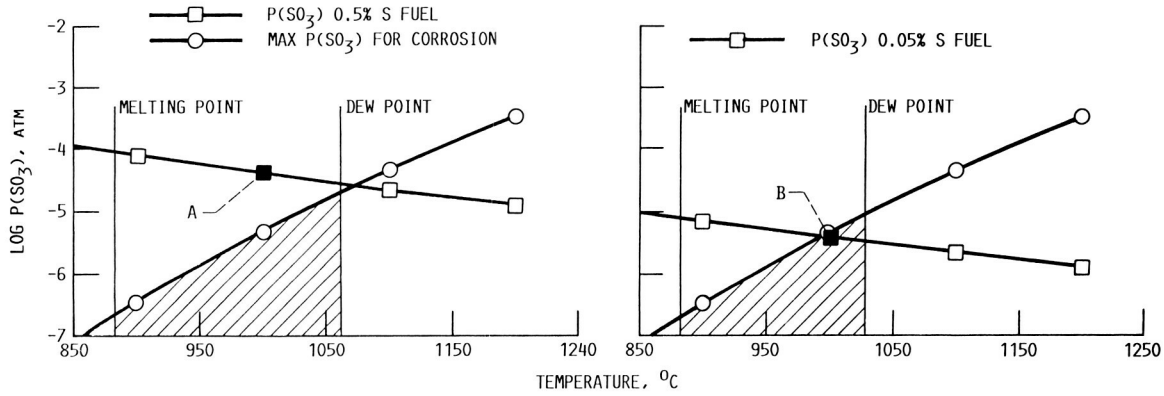

(A) NUMBER 2 DIESEL FUEL. (B) JET A FUEL.

FIGURE 1. - CALCULATED CORROSION REGIME (SHADED AREA) FOR SiO_2 AS A FUNCTION OF TEMPERATURE AND SO_3 PARTIAL PRESSURE FOR (A) NUMBER 2 DIESEL FUEL AND (B) JET A FUEL. WITH NUMBER 2 DIESEL FUEL, THE $P(SO_3)$ LINE DOES NOT INTERSECT THE SHADED AREA AT 1000 °C (POINT A) - CORROSION DOES NOT OCCUR. WITH JET A FUEL, THE $P(SO_3)$ LINE INTERSECTS THE CORROSION REGIME AT 1000 °C (POINT B) - CORROSION DOES OCCUR. CORROSION OCCURS AT ALL TEMPERATURES WHERE THE $P(SO_3)$ LINE INTERSECTS THE SHADED AREA.

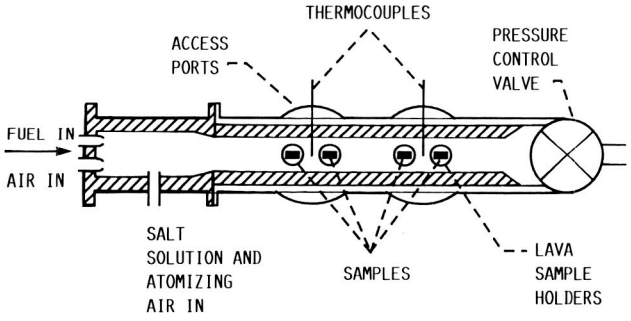

FIGURE 2. - SCHEMATIC OF NASA-LERC MACH 0.3 FOUR ATMOSPHERE BURNER RIG.

FIGURE 3. - CARBORUNDUM HEXOLOY SINTERED α-SiC EXPOSED FOR 40 H AT 1000 °C, 2 PPM Na, 400 kPa (AIR FLOW LEFT TO RIGHT).

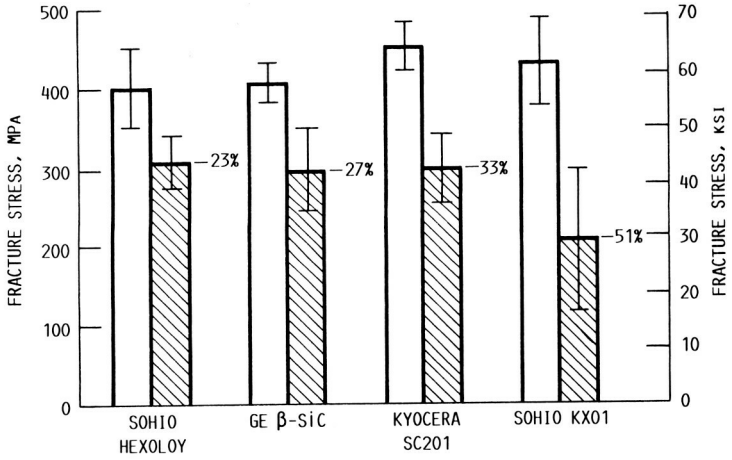

FIGURE 4. - ROOM TEMPERATURE FOUR-POINT BEND STRENGTH OF AS-RECEIVED AND CORRODED SILICON CARBIDE (40 H, 2 PPM Na, 1000 ^{O}C, 400 KPA PRESSURE).

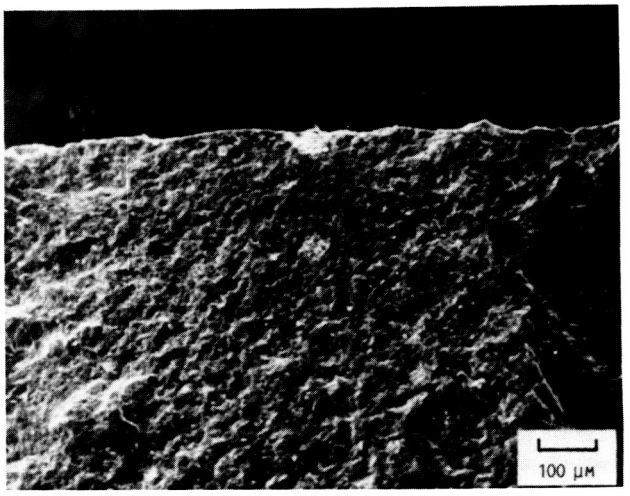

(A) CRACK LINES RADIATING FROM CORROSION PIT.

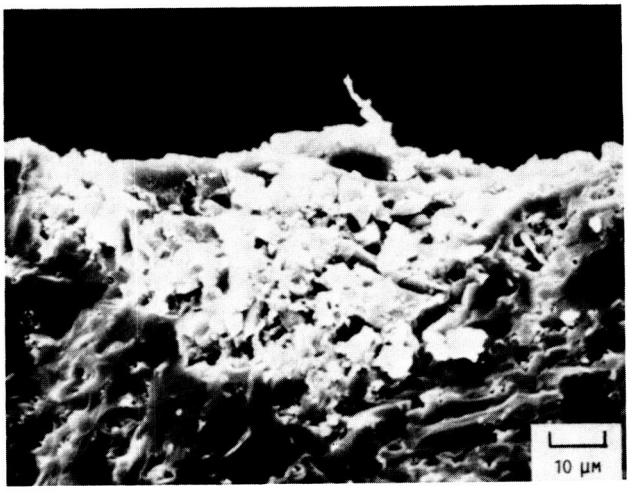

(B) ENLARGEMENT SHOWING GLASSY PRODUCT AT THE ORIGIN.

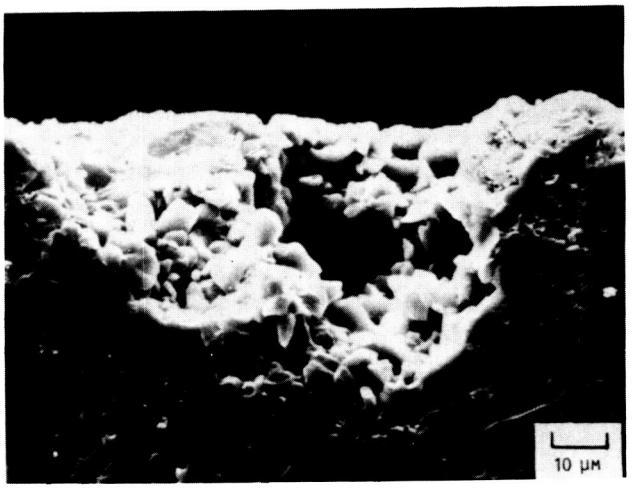

(C) PIT VISIBLE AFTER HF TREATMENT.

FIGURE 5. - FRACTURE ORIGIN AT LEADING EDGE OF CORRODED HEXOLOY α-SiC (σ = 341 MPA).

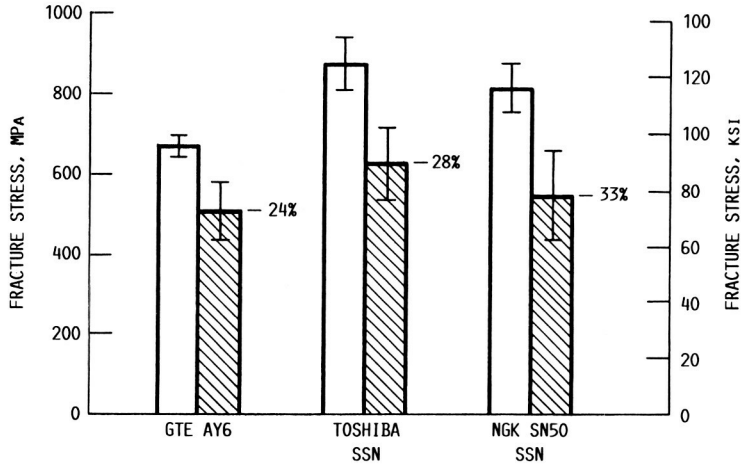

FIGURE 6. - ROOM TEMPERATURE FOUR-POINT BEND STRENGTH OF AS-RECEIVED AND CORRODED SILICON NITRIDE (40 H, 2 PPM Na, 1000 ^{0}C, 400 KPA PRESSURE).

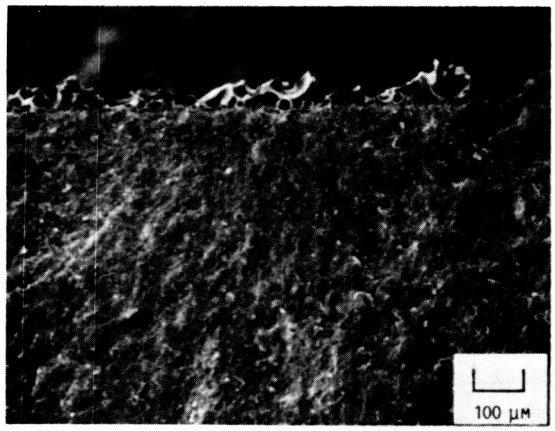

(A) CRACK LINES RADIATING FROM CORROSION PIT.

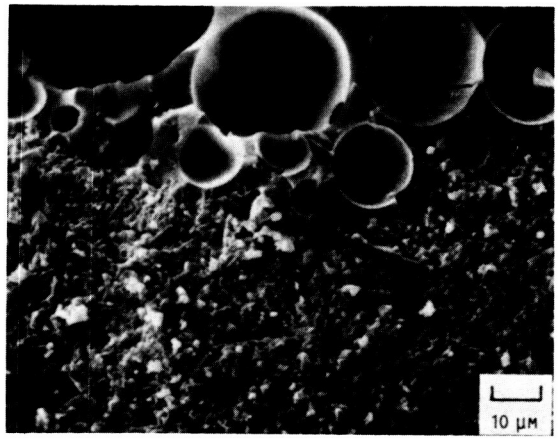

(B) ENLARGEMENT OF CORROSION PRODUCT AND BUBBLES IN THE PIT.

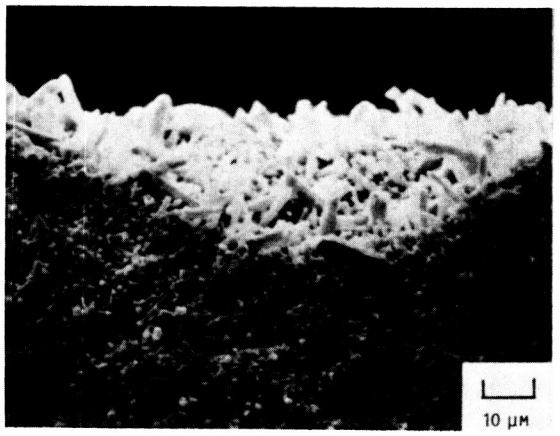

(C) PIT REVEALED AFTER HF TREATMENT.

FIGURE 7. - TRAILING EDGE FRACTURE ORIGIN OF CORRODED GTE AY6 Si_3N_4 (σ = 624 MPA).

FIGURE 8. - CORDIERITE EXPOSED FOR 40 H AT 1000 ^{0}C, 2 PPM Na, 400 KPA (AIR FLOW RIGHT TO LEFT).

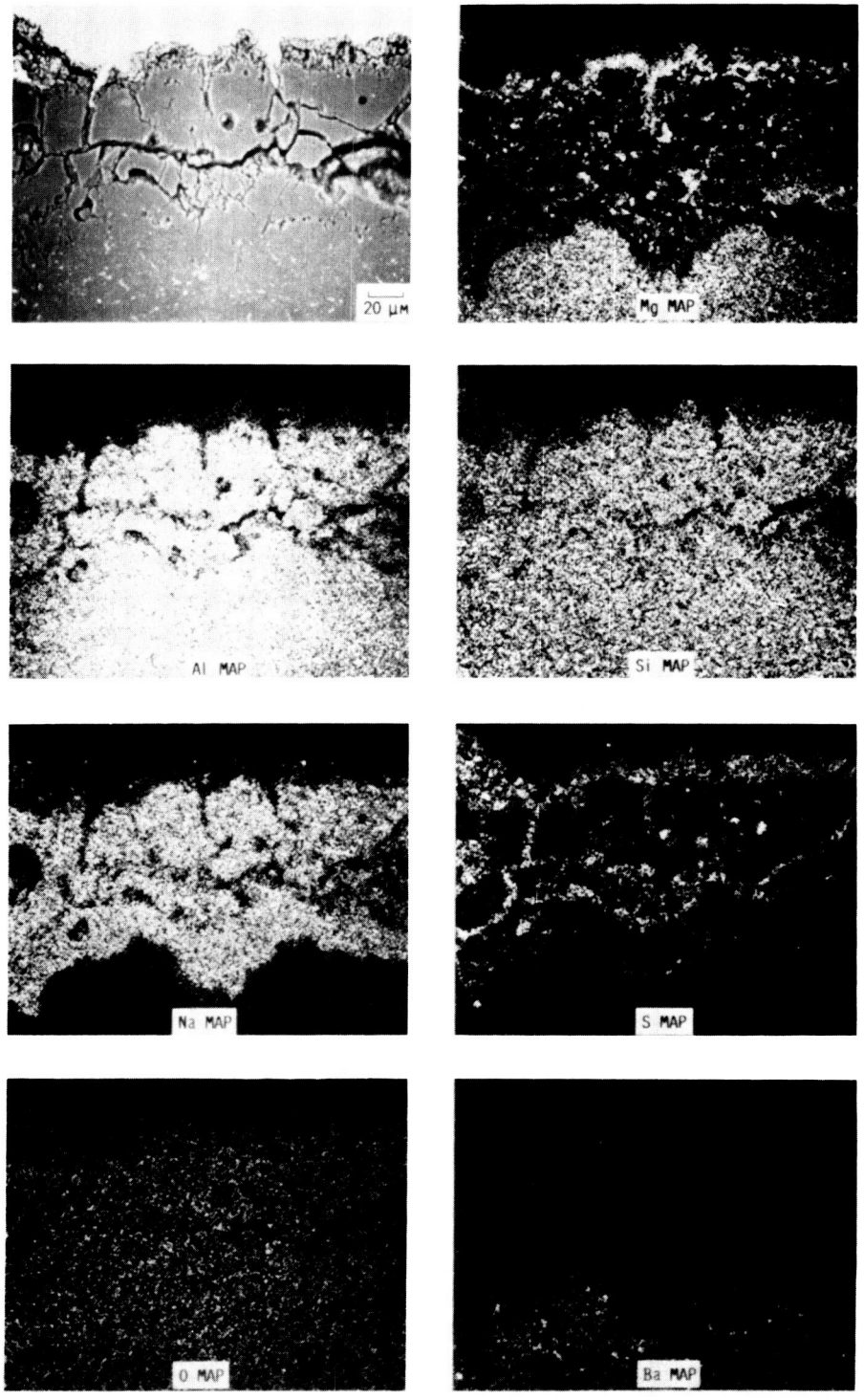

FIGURE 9. - POLISHED CROSS SECTION AND ASSOCIATED ELEMENTAL DOT MAPS FOR THE MIDDLE CORDIERITE SPECIMEN IN FIGURE 8.

NASA
National Aeronautics and Space Administration

Report Documentation Page

1. Report No.	2. Government Accession No.	3. Recipient's Catalog No.
NASA TM-101439 DOE/NASA/50111-2		

4. Title and Subtitle	5. Report Date
Hot Corrosion of Ceramic Engine Materials	6. Performing Organization Code

7. Author(s)	8. Performing Organization Report No.
Dennis S. Fox, Nathan S. Jacobson, and James L. Smialek	E-4544
	10. Work Unit No. 778-32-11

9. Performing Organization Name and Address	11. Contract or Grant No.
National Aeronautics and Space Administration Lewis Research Center Cleveland, Ohio 44135-3191	13. Type of Report and Period Covered Technical Memorandum
12. Sponsoring Agency Name and Address	14. Sponsoring Agency Code
U.S. Department of Energy Office of Vehicle and Engine R&D Washington, D.C. 20545	

15. Supplementary Notes

Final Report. Prepared under Interagency Agreement DE-AI01-85CE50111. Prepared for the Twenty-sixth Automotive Technology Development Contractors' Coordination Meeting sponsored by the U.S. Department of Energy, Dearborn, Michigan, October 24-27, 1988. (This effort was jointly sponsored by NASA and the U.S. Department of Energy.)

16. Abstract

A number of commercially available SiC and Si_3N_4 materials were exposed to 1000 °C in a high velocity, pressurized burner rig as a simulation of a turbine engine environment. Sodium impurities added to the burner flame resulted in molten Na_2SO_4 deposition, attack of the SiC and Si_3N_4, and formation of substantial Na_2O-x(SiO_2) corrosion product. Room temperature strength of the materials decreased. This was a result of the formation of corrosion pits in SiC, and grain boundary dissolution and pitting in Si_3N_4. Corrosion regimes for such Si-based ceramics have been predicted using thermodynamics and verified in rig tests of SiO_2 coupons. Protective mullite coatings are being investigated as a solution to the corrosion problem for SiC and Si_3N_4. Limited corrosion occurred to cordierite ($Mg_2Al_4Si_5O_{18}$), but some cracking of the substrate occurred.

17. Key Words (Suggested by Author(s))	18. Distribution Statement
Corrosion Silicon carbide Silicon nitride Molten salts	Unclassified – Unlimited Subject Category 27 DOE Cateogory UC 25

19. Security Classif. (of this report)	20. Security Classif. (of this page)	21. No of pages	22. Price*
Unclassified	Unclassified	16	A03

NASA FORM 1626 OCT 86

*For sale by the National Technical Information Service, Springfield, Virginia 22161